J. Ritman*, O. I. Yuldashev, M. B. Yuldasheva

AN ALGORITHM FOR CONSTRUCTION
OF DIPOLE MAGNETS COMPUTER MODELS
WITH QUALITY CONTROL AND ITS APPLICATION
FOR THE **PANDA** FORWARD SPECTROMETER

*Institute for Nuclear Physics, Juelich, Germany

Ритман Д., Юлдашев О. И., Юлдашева М. Б.   E11-2005-49

Алгоритм построения компьютерных моделей
дипольных магнитов с контролем точности
и его применение для переднего спектрометра PANDA

Представлен алгоритм создания компьютерных моделей дипольных магнитов спектрометров с заданными параметрами. Он состоит из следующих шагов: 1) получение аналитических оценок для ампер-витков, длины магнита и толщины ярма; 2) построение компьютерной модели обмотки и формирования ярма магнита; 3) оценка точности компьютерной модели; 4) получение характеристик магнита.

В предлагаемом алгоритме используются следующие входные параметры: поворотная сила магнита, рабочая область, тип стали и материал проводника. В качестве примера применения рассматривается задача построения компьютерной модели диполя для эксперимента PANDA в GSI (Дармштадт).

Ritman J., Yuldashev O. I., Yuldasheva M. B.   E11-2005-49

An Algorithm for Construction of Dipole Magnets
Computer Models with Quality Control and Its Application
for the PANDA Forward Spectrometer

This paper presents an algorithm for creating computer models of spectrometer dipole magnets with required parameters. It contains the following steps: 1) analytical estimates for ampere turns, magnet length and yoke thickness; 2) construction of a computer model for the coil and formation of the magnet yoke; 3) quality control of the computer model; 4) output of obtained magnet characteristics.

The following input parameters are used in the proposed algorithm: the magnet bending power, the magnet working region, steel type and conductor material. As an example of its application we consider the problem of creation of the computer dipole model for the PANDA experiment at GSI (Darmstadt).

INTRODUCTION

The main requirements to spectrometer dipole magnets usually are a magnitude of the magnet's bending power, a volume of working region, operating conditions, a conductor material and a steel type. Based on the input parameters, the process of the computer dipole model development can be described by the algorithm:

1) estimate the ampere turns, the magnet length and the yoke thickness by means of analytical formulas;

2) construct a computer model for the coil and form a geometry of the magnet yoke;

3) analyze the quality of the developed computer model;

4) calculate the most important magnet characteristics, for example:

— functions of the field along the rays in the polar coordinate system centered in the interaction point to estimate the bending power;

— field behavior in the iron to estimate saturation effects;

— body forces and torques acting on conductors with using the formula: $\mathbf{J} \times \mathbf{B}$;

— field behavior around the magnet;

— stored energy;

— forces acting on the magnetic parts (Maxwell stress) and others.

As an example of the algorithm application, we consider the problem of creating the computer dipole model for the PANDA experiment at GSI, Darmstadt.

The main requirements to the dipole magnet of the PANDA Forward Spectrometer are the following:

— the magnet bending power should be greater than 1.5 T·m and less or equal to 2 T·m;

— the acceptance angles are ± 5 degrees in vertical plane and ± 10 degrees in horizontal plane in the polar coordinate system with the centre outstanding from the magnet at the distance of 3.5 m;

— it is desirable to use standard materials for steel and conductor.

There is an additional condition: the magnet length must be greater or equal to 2 m and less or equal to 2.5 m. It was also suggested to introduce an iron plate into the dipole to protect a beam against the magnetic field. The iron plate should have 10 cm in thickness and the full width of the dipole in other two directions. The beam channel of 7–8 cm in diameter inside the plate is presupposed.

1

In accordance with these requirements, a computer dipole magnet model with iron plate (Fig. 1) has been constructed and presented by the authors at the PANDA collaboration meeting, INP (Juelich), 29 November – 1 December 2004.

Let us describe all steps of the algorithm.
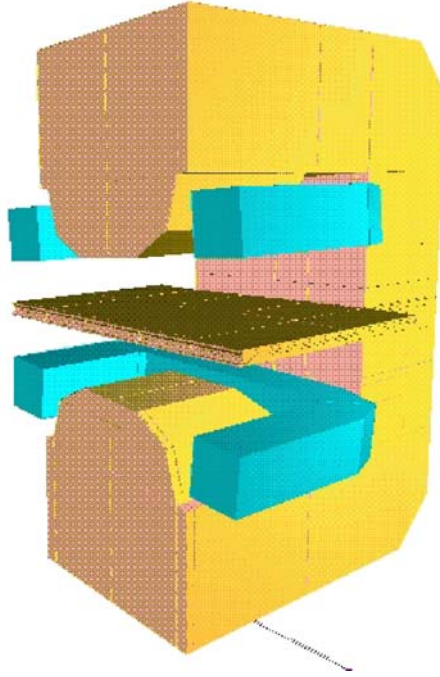
Fig. 1. Computer dipole model for the PANDA (1/2 symmetrical part)

1. ANALYTICAL ESTIMATES FOR AMPERE TURNS, MAGNET LENGTH AND YOKE THICKNESS

We use static Maxwell's equations in the form

$$\nabla \cdot \mathbf{B} = 0, \quad \nabla \times \mathbf{H} = 0, \quad \mathbf{B} = \mu_0 \mu \mathbf{H}$$

for a magnetic region,

$$\nabla \cdot \mathbf{B} = 0, \quad \nabla \times \mathbf{H} = \mathbf{J}, \quad \mathbf{B} = \mu_0 \mathbf{H}$$

for a nonmagnetic region, and

$$[\mathbf{B} \cdot \mathbf{n}] = 0, \quad [\mathbf{H} \times \mathbf{n}] = 0$$

for a boundary between the two regions, where $\mathbf{B}, \mathbf{H}, \mathbf{J}$ are magnetic flux density, field intensity and current density, respectively; μ is a function of magnetic permeability; and μ_0 is the magnetic constant. For simplicity we assume that in the Cartesian coordinate system the magnet center has zero coordinates, and B_y is the main field component. Let us estimate the magnet length and ampere turns using such an information about the magnet as the given bending power and the volume of the working region. We will presuppose that operation conditions of the magnet permit one to apply low carbon steel 3 and that the permissible level of average yoke saturation is less than 1.5 T.

From the equations mentioned above and from the Gauss theorem about circulation we have

$$\int_L \mathbf{H} \cdot \mathbf{dl} = 2 \cdot J_z, \tag{1}$$

where L is a closed contour (see Fig. 2 or Fig. 3).
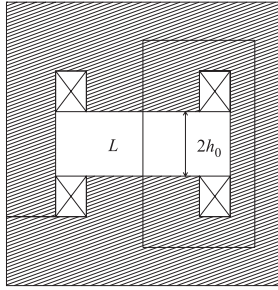
Fig. 2. Cross section of a magnet with coil placement of the first type
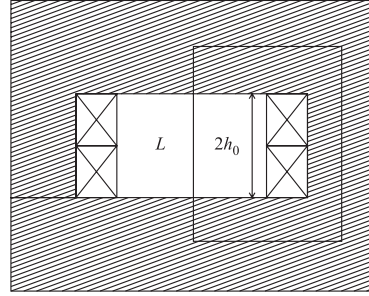
Fig. 3. Cross section of a magnet with coil placement of the second type

Due to the symmetry and construction peculiarities of the dipole magnets from Eq. (1) we obtain

$$\frac{1}{\mu_0} B_0 h_0 \approx J_z,$$

where B_0 is the field in the magnet center. If C denotes the current density and S_C is the area of the coil cross section, then

$$J_z = C S_C$$

3

and

$$B_0 \approx \frac{\mu_0}{h_0} C S_C = \frac{\mu_0}{h_0} C x^2. \tag{2}$$

Here for simplicity we presuppose that $S_C = x^2$. Let d be a magnet length. For the bending power $\hat{B}$ we have

$$\int_{-d/2+x}^{d/2-x} B_y dz = \hat{B}.$$

From approximate formula

$$\hat{B} = \int_{-d/2+x}^{d/2-x} B_y dz \approx B_0 \cdot (d - 2x)$$

and from Eq. (2) we obtain the following cubic equation:

$$B_0^3 - \left(\frac{C\mu_0}{4h_0}\right) d^2 B_0^2 + \left(\frac{C\mu_0}{4h_0}\right) 2d\hat{B}B_0 - \left(\frac{C\mu_0}{4h_0}\right) \hat{B}^2 = 0. \tag{3}$$

The approximate solutions of Eq. (3) are presented in Table 1 for the following values of parameters: $C = 220$ A/cm^2, $h_0 = 0.5$ m, $\hat{B} = \sigma \cdot 2(\text{T} \cdot \text{m})$, $\sigma = 0.8, 0.9, 0.95, 1.0$, $d = 2.0, 2.1, 2.2, \ldots, 3.2$ m.

Table 1

	d (m)	2.0	2.1	2.2	2.3	2.4	2.5	2.6
$\sigma = 0.8$	B_0 (T)	1.99	1.52	1.30	1.15	1.04	0.96	0.89
	x (m)	0.60	0.52	0.48	0.46	0.43	0.42	0.40
$\sigma = 0.9$	B_0 (T)	—	—	1.60	1.39	1.24	1.13	1.04
	x (m)	—	—	0.54	0.50	0.47	0.45	0.43
$\sigma = 0.95$	B_0 (T)	—	—	1.79	1.52	1.34	1.22	1.12
	x (m)	—	—	0.57	0.52	0.49	0.47	0.45
$\sigma = 1.0$	B_0 (T)	—	—	—	1.66	1.46	1.31	1.20
	x (m)	—	—	—	0.55	0.51	0.49	0.47

	d (m)	2.7	2.8	2.9	3.0	3.1	3.2
$\sigma = 0.8$	B_0 (T)	0.83	0.78	0.74	0.70	0.67	0.63
	x (m)	0.39	0.38	0.37	0.36	0.35	0.34
$\sigma = 0.9$	B_0 (T)	0.97	0.90	0.85	0.80	0.76	0.73
	x (m)	0.42	0.40	0.39	0.38	0.37	0.36
$\sigma = 0.95$	B_0 (T)	1.03	0.97	0.91	0.86	0.81	0.78
	x (m)	0.43	0.42	0.41	0.39	0.38	0.37
$\sigma = 1.0$	B_0 (T)	1.11	1.03	0.97	0.91	0.87	0.82
	x (m)	0.45	0.43	0.42	0.41	0.40	0.30

4

For $\sigma = 0.9, 0.95, 1.0$, $d = 2, 2.1$ m and $\sigma = 1.0$, $d = 2.2$ m the equation has no solutions.

Table 1 shows that $B_0 \approx 2$ T for $\sigma = 0.8$ and $d = 2$ m (bending power is about 1.6 T·m). If we use the steel with magnetic characteristic from Fig. 4, then the permissible level of the field entering the pole is less than 1.5 T. Therefore, we should use $d > 2$ m.
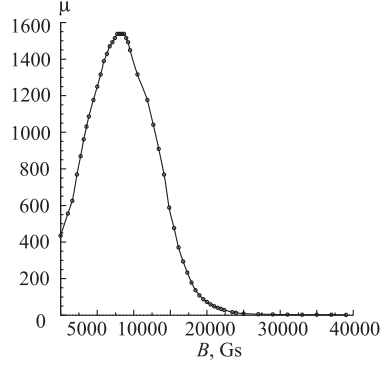

Fig. 4. The magnetic characteristic $\mu(|\mathbf{B}|)$ for steel 3
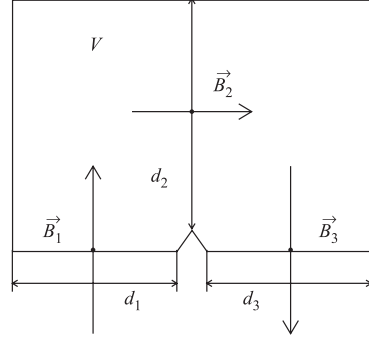
Fig. 5. The flux rotation in volume V

Let us estimate the thickness of the iron yoke using the magnetic steel characteristic. Presuppose that the magnetic flux rotates in the yoke as in Fig. 5 and $B_z \approx 0$. Then from the formula

$$\int\limits_V \nabla \cdot \mathbf{B}\, dV = \int\limits_{\partial V} \mathbf{B} \cdot \mathbf{n}\, dS,$$

where $\mathbf{n}$ is an outward normal vector, we obtain the approximations

$$B_{1,y}d_1 \approx B_{2,x}d_2, \quad B_{2,x}d_2 \approx -B_{3,y}d_3.$$

Since $\mathbf{B}_1$ is the field entering the pole and d_1 is defined by the volume of a working region, we can estimate d_2, d_3 choosing $B_{2,x}, B_{3,y}$ from the permissible level of a yoke saturation. Futher the obtained estimates are an additional input information for the next step of the algorithm.

2. CONSTRUCTION OF A COMPUTER MODEL FOR THE COIL AND FORMATION OF THE MAGNET YOKE

Resistive coils are usually used for spectrometer dipole magnets in view of their simple construction. The so-called «racetrack», «bedstead» coil types and

5

the coil wound on the surface of a cylinder are widely spread but they are not optimal for the class of spectrometers with a magnet working region in the form of a truncated pyramid or a cone. In this case for the coil description we have to take into account that the coil should be placed around the working region and it is useful to introduce special angles φ, θ, ψ which describe rotations of a point $x = (x_1, x_2, x_3)$ around the coordinate axes according to formulas [1]:

$$A_1(\varphi) = \begin{pmatrix} \cos\varphi & -\sin\varphi & 0 \\ \sin\varphi & \cos\varphi & 0 \\ 0 & 0 & 1 \end{pmatrix}, \quad A_2(\theta) = \begin{pmatrix} \cos\theta & 0 & \sin\theta \\ 0 & 1 & 0 \\ -\sin\theta & 0 & \cos\theta \end{pmatrix},$$

$$A_3(\psi) = \begin{pmatrix} 1 & 0 & 0 \\ 0 & \cos\psi & -\sin\psi \\ 0 & \sin\psi & \cos\psi \end{pmatrix}.$$

If we calculate the coil field $\mathbf{B}^S$ by the Biot–Savart's law

$$\mathbf{B}^S(x) = \frac{\mu_0}{4\pi} \sum_{i=1}^{n} \int_{\Omega_{S,i}} \mathbf{J}_i(y) \times \nabla_y \frac{1}{|x-y|} d\Omega_y,$$

where $\Omega_{S,i}$ $(i = 1, \ldots, n)$ are the coil elements, $|x - y|$ is the distance between points x and y, then we have

$$\mathbf{B}^S(x) = \frac{\mu_0}{4\pi} \sum_{i=1}^{n} \int_{\Omega_{S,i}} A_i \mathbf{J}_i(y') \times A_i \nabla_{y'} \frac{1}{|x-y'|} d\Omega_{y'}, \qquad (4)$$

where $A_i = A_1(\varphi_i) A_2(\theta_i) A_3(\psi_i)$ and y' belongs to ith local coordinate system in which ith coil element has a simple geometry. In view of the conditions $\nabla \cdot \mathbf{B}^S = 0$ and $\nabla \times \mathbf{B}^S = \mathbf{J}$ in the next section we shall discuss how to control the accuracy of computations with formula (4).

The area of the coil cross section depends on a chosen conductor material (usually copper or aluminum) and a cooling method. Figure 6 shows a top view of the coil model which may be used for the PANDA dipole. Figure 7 presents the coil field for plane $y = 0$ calculated with using the estimates for ampere turns.

In order to construct an additional iron field, we use the Maxwell's equations with substitutions: $\mathbf{H} = \nabla u$ for magnetic regions and $\mathbf{H} = \nabla v + \mathbf{B}^S/\mu_0$ for air regions. As a result, we have the mathematical model [2]

$$\nabla \cdot \mu \nabla u = 0 \qquad (5)$$

for a magnetic region,

$$\nabla \cdot \nabla v = 0 \qquad (6)$$

6
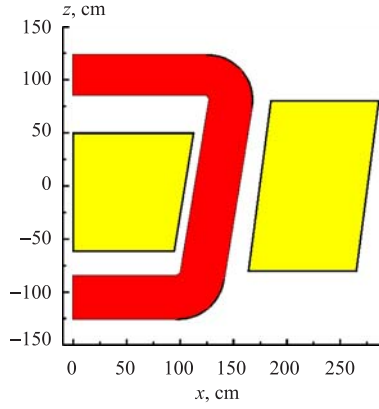
Fig. 6. The magnet cross section by the plane $y = 0.7$ m for $x \geqslant 0$
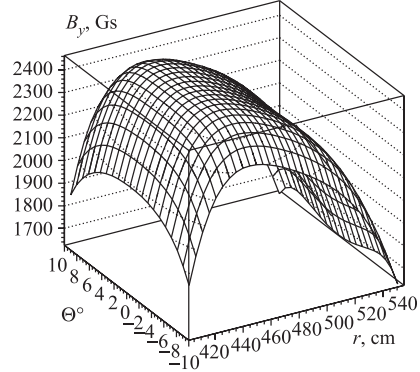
Fig. 7. The coil field in working region for plane $y = 0$

for a nonmagnetic region, with boundary conditions between the two regions

$$
\mu(\partial u/\partial n) = \partial v/\partial n + \mathbf{n} \cdot \mathbf{B}^S/\mu_0,
$$
$$
u = v + v^S,
\tag{7}
$$

and with condition $v = 0$ at infinity points. Here v^S is defined by equations [3]:

$$
(\nabla v^S - \mathbf{B}^S/\mu_0) \times \mathbf{n} = 0,
$$
$$
v^S(x_0) = 0,
\tag{8}
$$

where x_0 belongs to the boundary. If μ is a constant, then we have a linear problem and for $\mu = \mu(|\nabla u|)$ we obtain a nonlinear case.

Use an iterative process for yoke formation. As a starting point of the process, a space around the coil is filled by iron in accordance with the analytical estimates and Figs. 2, 3. Further the following procedure is carried out step by step:

1) for all elements ω_i, $i = 1, \ldots, k$ in iron: calculate $|\mathbf{B}_i|$ in the middle point of the ith element;

2) for all elements in iron ($1 \leqslant i \leqslant k$): if $|\mathbf{B}_i|$ is greater than the permissible field level for iron yoke saturation, then the element ω_i is filled by air;

3) if the yoke geometry has been changed in such a way, we repeat steps 1 and 2, otherwise the yoke formation process is finished.

On the final stage the obtained yoke configuration should be considered from the point of manufacturing simplicity.

7

Distribution of |B|(Gs) in yoke

16963.0 15000 7740.71 81.4094
17944.6 15981.5 11370.35 4111.06

Distribution of |B|(Gs) in yoke

11301.2 7669.28 4037.31 405.348
13117.2 9485.26 5853.29 2221.33
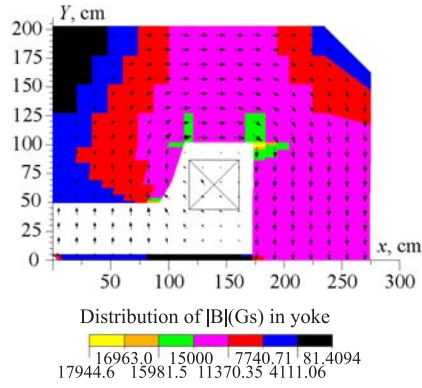
Fig. 8. Distribution of $|\mathbf{B}|$ in yoke and field behavior for plane $z = 0$ and $x,\ y \geqslant 0$
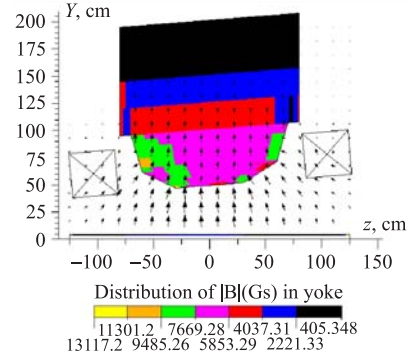
Fig. 9. Distribution of $|\mathbf{B}|$ in yoke and field behavior for plane $x = 0$ cm and $y \geqslant 0$

Table 2 and Figs. 8, 9 show the distribution of $|\mathbf{B}|$ in the iron yoke of the PANDA dipole model.

Table 2. The magnet parts saturation

Part	V, cm^3	$\dfrac{1}{|V|}\displaystyle\int_V |\mathbf{B}|dV$, T
Front part of the pole	$0 \leqslant x \leqslant 100.625$ $47.0625 \leqslant y \leqslant 91.5$ $-70 \leqslant z \leqslant 0$	1.0124
Back part of the pole	$0 \leqslant x \leqslant 123.75$ $49.5 \leqslant y \leqslant 97.1875$ $0 \leqslant z \leqslant 70$	0.9782
Upper beam	$99 \leqslant x \leqslant 175$ $85 \leqslant y \leqslant 198$ $-80 \leqslant z \leqslant 80$	1.3474
Side wall	$149 \leqslant x \leqslant 276$ $0 \leqslant y \leqslant 98$ $-80 \leqslant z \leqslant 80$	1.3798
Plate	$0 \leqslant x \leqslant 175$ $0 \leqslant y \leqslant 5$ $-125 \leqslant z \leqslant 125$	0.5360

8

Figure 10 presents the average field integral S_A as a relative current function. This dependence is an important characteristic of the magnet model and it is a linear function in case of a nonsaturated magnet.

In Table 3 and Fig. 10

$$S_{A,i} = \frac{1}{n_x \cdot n_y} \sum_{k=1}^{n_x} \sum_{m=1}^{n_y} \int_{L_{km}} B_{y,i} dL,$$

$$L_{km} = \left\{ x = \left(k - \frac{1}{2} \right) \tan 10° \cdot 6.8 \text{ m}/n_x; \right.$$

$$y = \left(m - \frac{1}{2} \right) \tan 5° \cdot 6.8 \text{ m}/n_y;$$

$$\left. 0 \leqslant z \leqslant 6.8 \text{ cm} \right\} \quad k = 1, 2, \ldots n_x, \quad m = 1, 2, \ldots n_y,$$

where $n_x = 48$, $n_y = 24$, $B_{y,i}$ is the field obtained with current I_i,

$$S_{A,i}^* = \frac{I_i}{I_1} \cdot S_{A,1},$$

and I_0 is the nominal current.
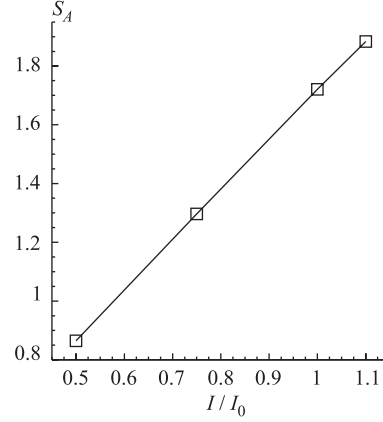
Fig. 10. Average integral S_A as a relative current I/I_1 function

Table 3

i	1	2	3	4
I_i	$0.5I_0$	$0.75I_0$	I_0	$1.1I_0$
$S_{A,i}$ (T)	0.8647	1.2966	1.7207	1.8833
$S_{A,i}^*$ (T)	0.8647	1.2971	1.7294	1.9024
$|S_{A,i} - S_{A,i}^*|$ (T)	0	0.0005	0.0088	0.0191

Figure 10 and Table 3 show that the average integral S_A (bending power) and the extrapolated integral $S_{A,i}^*$ have practically a linear dependence on current in the coil. Therefore, under the nominal current the iron yoke saturation is not observed on the whole in the presented magnet model.

3. QUALITY CONTROL OF THE COMPUTER MODEL

When solving the magnetostatic problems by the finite element method, we obtain generalized numerical solutions. Under the correct application of the method on a sequence of condensed meshes we have a sequence of approximate solutions convergents to the exact solution of the problem. The accuracy of numerical solutions of mathematical model (5)–(7) depends on both the accuracy of calculation of the vector $\mathbf{B}^S$ by formula (4) and the accuracy of solving the mesh problem. Let us regard possible reasons of the errors arising when calculating the vector $\mathbf{B}^S$. The first one is in piecewise constant approximation of the vector $\mathbf{J}$ for every element of the coil.

Define $\Omega_S = \sum\limits_{i=1}^{n} \Omega_{S,i}$. Then we have

$$
\frac{1}{\mu_0}\nabla \times \mathbf{B}^S(x) = \nabla \times \nabla \times \int\limits_{\Omega_S} \frac{\mathbf{J}}{4\pi|x-y|}d\Omega_y = \nabla\left(\nabla \int\limits_{\Omega_S}\frac{\mathbf{J}}{4\pi|x-y|}d\Omega_y\right) -
$$

$$
-\nabla^2\int\limits_{\Omega_S}\frac{\mathbf{J}}{4\pi|x-y|}d\Omega_y = \nabla\sum_{i=1}^{n}\left(\int\limits_{\Omega_{S,i}}\frac{\nabla\cdot\mathbf{J}_i}{4\pi|x-y|}d\Omega_y - \int\limits_{\partial\Omega_{S,i}}\frac{\mathbf{J}\cdot\mathbf{n}}{4\pi|x-y|}d\Omega_y\right) + \mathbf{J}.
$$

From here we obtain the condition

$$
[\mathbf{J}_i \cdot \mathbf{n}] = 0, \quad y \in \partial\Omega_{S,i}, \quad i = 1, 2, \cdots, n.
$$

Under this condition $(1/\mu_0)\nabla \times \mathbf{B}^S = \mathbf{J}$.

Second, errors in calculations of the vector $\mathbf{B}^S$ appear under integration by means of cubature formulas. These errors are connected with the limited accuracy of the cubature formulas and with the restricted accuracy of the isoparametric transformation [4] used as a rule for mapping, for example, a hexahedron into the unit cube.

To test the correctness of the vector $\mathbf{B}^S$ calculation, it is possible to use the finite-difference operators in the form

$$
D_{ij}^h\mathbf{B}^S(x) = (B_i^S(x_j + h) - B_i^S(x_j))/h, \quad 1 \leqslant i,j \leqslant 3,
$$

where h is a parameter. Finite-difference operators $\nabla^h\cdot$ and $\nabla^h\times$ can be constructed from these operators. As it follows from the approximation theory, for the $\mathbf{B}^S$ calculated correctly we have to obtain the following two sequences:

$$
\nabla^h \cdot \mathbf{B}^S(x), \nabla^{h/2} \cdot \mathbf{B}^S(x), \ldots, \nabla^{h/m} \cdot \mathbf{B}^S(x),
$$

$$
\nabla^h \times \mathbf{B}^S(x), \nabla^{h/2} \times \mathbf{B}^S(x), \ldots, \nabla^{h/m} \times \mathbf{B}^S(x),
$$

which converge to corresponding exact values.

10

At the beginning of the model construction process we usually solve linear and nonlinear problems on rough meshes. The necessity to obtain a more precise model is connected with mesh refinement. There are some approaches for a quality control of the model for the magnetic system [5]. We use two a posteriori estimates in terms of characteristics η_i and θ_i.

The first one is useful to check how the solutions satisfy the Maxwell's equations in a classical sense [6]. For the reason we apply the local error indicator η_i [7] in the air region

$$\eta_i = \frac{1}{|w_i|} \left(|\int_{w_i} \frac{\nabla \times \mathbf{B}^{f,2}}{|\mathbf{B}^{f,1}(y_i)|} dw| + |\int_{w_i} \frac{\nabla \cdot \mathbf{B}^{f,2}}{|\mathbf{B}^{f,1}(y_i)|} dw| \right), \tag{8}$$

where

$$\mathbf{B}^{f,1}(x) = \mu_0 \sum_{j=1}^{8} \zeta_j \nabla N_j^{(1)}(x), \quad \mathbf{B}^{f,2}(x) = \mu_0 \sum_{k=1}^{27} \zeta_k \nabla N_k^{(2)}(x).$$

Here ζ_j, ζ_k are potential values in points x_j, x_k. They have been obtained by solving the problem with linear base functions on some mesh; $N_j^{(1)}$, $N_k^{(2)}$ are base functions of linear and quadratic elements, respectively; y_i is the middle point of element w_i; $|w_i|$ denotes the volume of w_i. It should also be noted that we have used the same characteristic η_i for testing the magnetic field functions based on measured data [7].

For iron region this local error indicator has another form in view of the constant piecewise approximation for function $\mu = \mu(|\mathbf{H}|)$. In fact, $\nabla \times \mathbf{B}^{f,2} = 0$ in air due to the property of operator $\nabla \times$ so this term can be omitted. We have the same situation in the iron region for $\mathbf{H} = \nabla u$. Therefore, for iron η_j can be defined by the formula

$$\eta_j = \frac{1}{|\hat{w}_j|} \left(|\int_{\hat{w}_j} \frac{\nabla \cdot \mathbf{B}^{\text{int},2}}{|\mathbf{B}^{\text{int},1}|} dw| \right),$$

where $\hat{w}_j$ is a hexahedron with the nodes obtained as the middle points of the elements which surround the jth mesh node inside the iron;

$$\mathbf{B}^{\text{int},2} = \sum_{m=1}^{8} \mathbf{B}_m N_m^{(1)}(x), \quad \mathbf{B}^{\text{int},1} = \frac{1}{8} \sum_{m=1}^{8} \mathbf{B}_m,$$

here $\mathbf{B}_m$ is the field in the same middle points.

11

The other local error indicator θ_i is useful to obtain a smooth (more correct) distribution of the calculated magnetic field. It has the form [8]:

$$\theta_i = \frac{1}{|w_i|} \int\limits_{w_i} \frac{|\mathbf{B}^{f,1} - \mathbf{B}^{f,2}|}{|B^{f,1}(y_i)|} dw.$$

Small values of θ_i point to the magnitude of discontinuities in the field vectors derived from the linear elements.

Table 4 presents η_i and θ_i for the calculated field.

Table 4. Quality characteristics of magnetic field calculations

Part	V, cm^3	$\frac{1}{n}\sum\limits_{i=1}^{n}\theta_i$, %	$\frac{1}{n}\sum\limits_{i=1}^{n}\eta_i$, %
Working region of the magnet	$0 \leqslant x \leqslant \tan 10°(z+475)$ $\tan 0.81°(z+475) \leqslant y \leqslant$ $\leqslant \tan 5.82°(z+475)$ $-180 \leqslant z \leqslant 180$	0.561	0.103
Front part of the pole	$0 \leqslant x \leqslant 100.625$ $47.0625 \leqslant y \leqslant 91.5$ $-70 \leqslant z \leqslant 0$	1.478	1.199
Back part of the pole	$0 \leqslant x \leqslant 123.75$ $49.5 \leqslant y \leqslant 97.1875$ $0 \leqslant z \leqslant 70$	2.458	1.152
Upper beam	$0 \leqslant x \leqslant 175$ $85 \leqslant y \leqslant 198$ $-80 \leqslant z \leqslant 80$	1.123	0.895
Side wall	$149 \leqslant x \leqslant 276$ $0 \leqslant y \leqslant 98$ $-80 \leqslant z \leqslant 80$	1.556	0.375
Region inside the channel	$0 \leqslant x \leqslant 3.5$ $0 \leqslant y \leqslant 3.5$ $-110 \leqslant z \leqslant 110$	0.032	0.052

Using the local error indicators is important when we want to be sure that the errors of approximate numerical solutions do not have an essential influence on the field behavior. An example of this situation is the calculated field inside the channel in the iron plate because the level of the magnetic field magnitude can be comparable with the level of approximation errors.

As is known from the results of the EXCHARM experiment [9], the characteristics η_i should be less than 1% [7]. In Table 4 this average characteristic

12
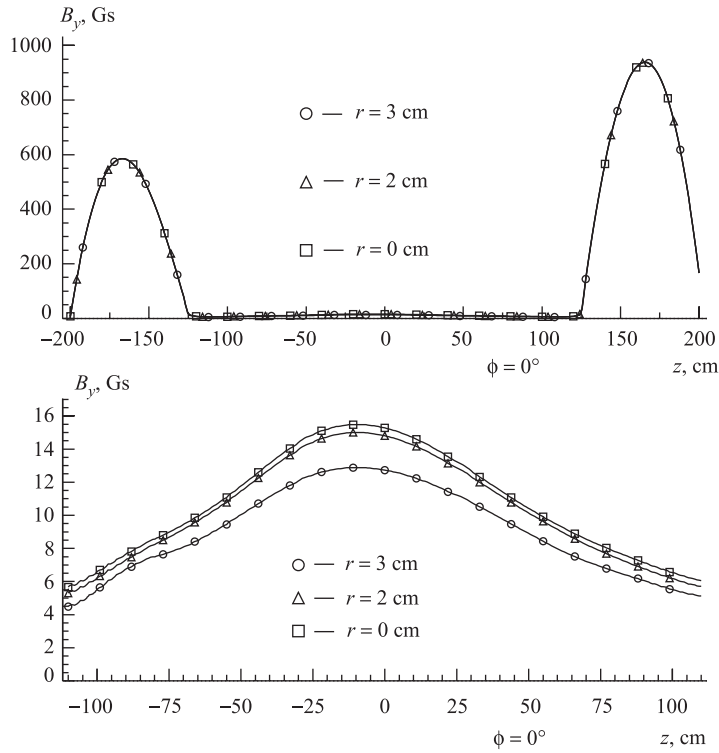
Fig. 11. The behavior of the main field component in the channel (polar coordinate system), $\varphi = 0°$

inside the channel of 7 cm in diameter is less than 0.052%. This result points to a sufficient good approximation used in the field calculation. Figure 11 shows the behavior of main field component in the channel.

4. OUTPUT OF OBTAINED MAGNET CHARACTERISTICS

Here we present some characteristics of the developed dipole model for the PANDA experiment. Figures 12–18 show the behavior of the field components along rays in the polar coordinate system (r, θ, φ) with the center at the point (–475;0;0). Table 5 gives the magnet bending power along the rays. Figure 19 presents the distribution of bending power homogeneity in the working region of the model. To prepare this picture, 1152 integrals have been calculated and we

13

finally conclude that the field integral homogeneity in 90% of the working region is less than 5%.
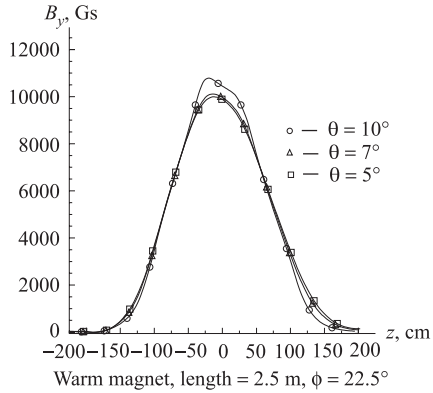
Fig. 12. The behavior of the main field component along rays in the polar coordinate system for $\varphi = 22.5°$
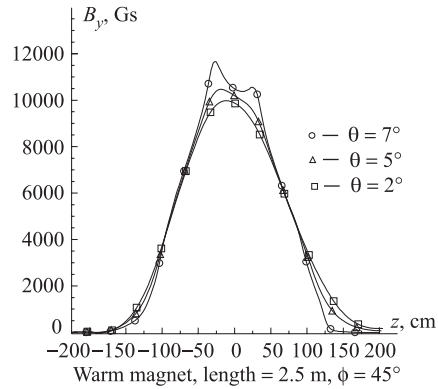
Fig. 13. The behavior of the main field component along rays in the polar coordinate system for $\varphi = 45°$
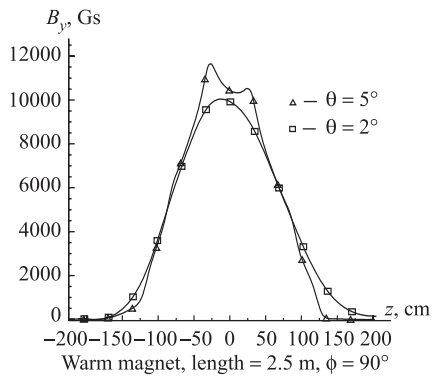
Fig. 14. The behavior of the main field component along rays in the polar coordinate system for $\varphi = 90°$
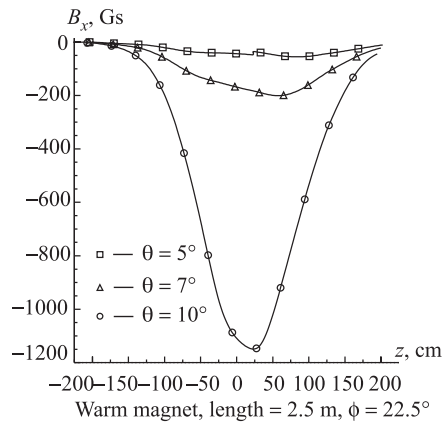
Fig. 15. The behavior of the B_x field component along rays in the polar coordinate system for $\varphi = 22.5°$

Figures 20, 21 give the distribution of $|\mathbf{B}|$ in the iron plate for two sections. These pictures show that under the nominal current the iron plate saturation is not observed.

14
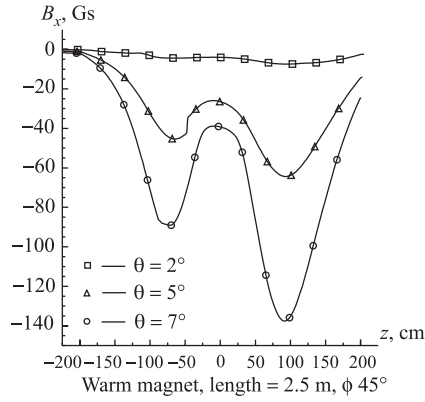
Fig. 16. The behavior of the B_x field component along rays in the polar coordinate system for $\varphi = 45°$
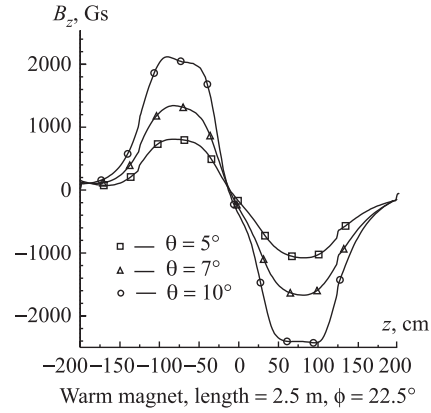
Fig. 17. The behavior of the B_z field component along rays in the polar coordinate system for $\varphi = 22.5°$

Table 5. The magnet bending power

$\int B_y dl$ (T · m)				
	$\theta = 2°$	$\theta = 5°$	$\theta = 7°$	$\theta = 10°$
$\varphi = 22.5°$	—	1.7119	1.7056	1.7227
$\varphi = 45°$	1.7185	1.7285	1.7443	—
$\varphi = 90°$	1.7215	1.7352	—	—
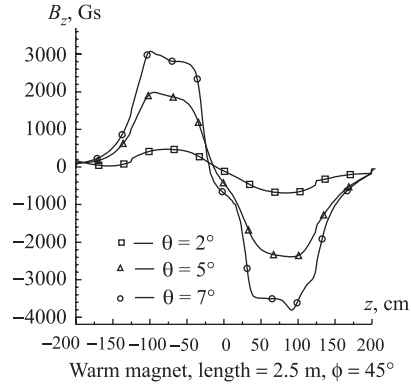
Fig. 18. The behavior of B_z field component along rays in polar coordinate system for $\varphi = 45°$

In Figs. 22, 23 the body forces acting on conductors are presented for symmetrical parts of the coil. The forces have been calculated in accordance with the formula

$$\mathbf{F}_i = \int\limits_{\Omega_{S,i}} \mathbf{J} \times \mathbf{B} d\Omega, \quad i = 1, \ldots 23,$$

where $\Omega_{S,i}$ is the enumerated part of the coil volume from Fig. 22.

15
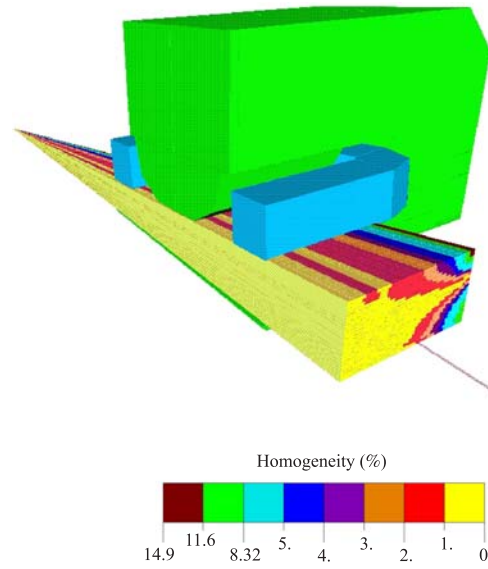
Fig. 19. Distribution of bending power homogeneity in the working region
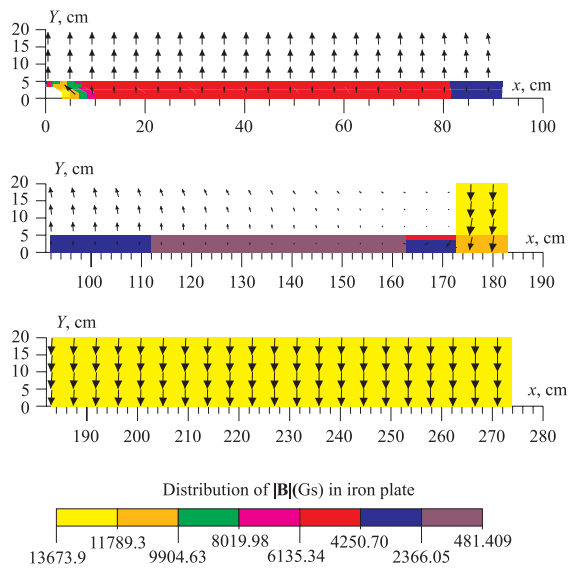
Fig. 20. Distribution of $|\mathbf{B}|$ in the iron plate and field behavior for plane $z = 0$ and $x, y > 0$

16
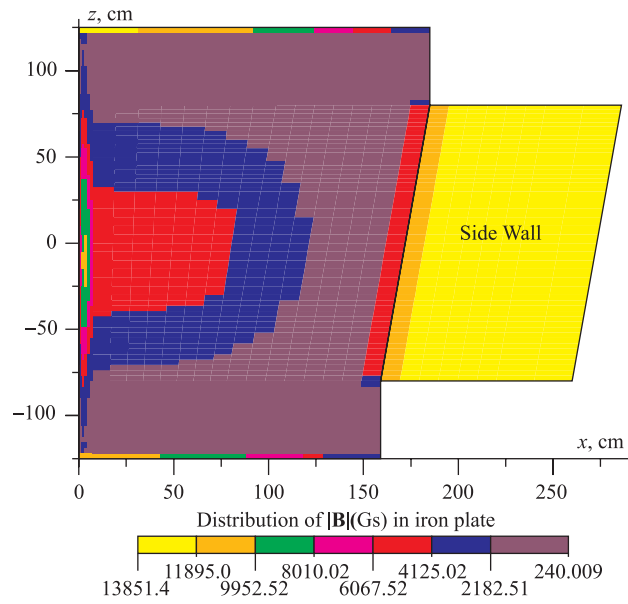
Fig. 21. Distribution of $|\mathbf{B}|$ in the iron plate for plane $y = 4.125$ cm and $x \geqslant 0$
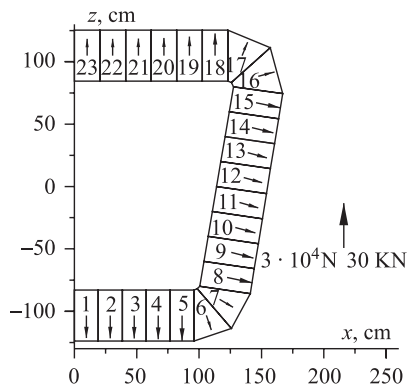

Fig. 22. Top view of the coil and force components $\mathbf{i}F_x + \mathbf{k}F_z$
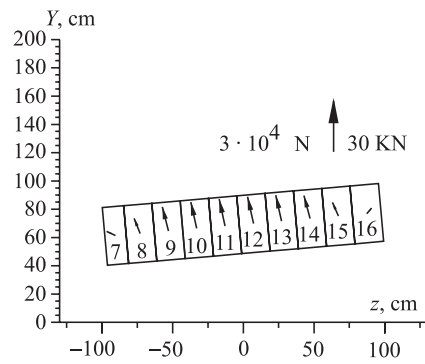
Fig. 23. Side view of the coil and force components $\mathbf{j}F_y + \mathbf{k}F_z$

17

CONCLUSION

We have described an algorithm for constructing dipole computer models with quality control of computations. We did not consider the question of field uniformity because it is a special problem. Note that some widely used computer aided design (CAD) programs intended for computation of 3D magnetic fields do not have the iterative loop to generate an iron yoke and do not have special routines for users to control the quality of magnet models. The suggested new characteristic η_i for the field quality control has two important advantages:

— it has a clear physical meaning because in essence it is the Maxwell equations in every finite element;

— it is a convenient tool for comparison of the calculated magnetic field functions, used for further simulations (for example, for tracking), with functions based on measured data.

All steps of the algorithm have been demonstrated for the PANDA dipole magnet model suggested by the authors in accordance with the requirements formulated in Introduction.

REFERENCES

1. *Korn G., Korn T.* Mathematical handbook for scientists and engineers. M.: Nauka, 1977 (in Russian).

2. *Simkin J., Trowbridge C. W.* Three-dimensional nonlinear electromagnetic field computations using scalar potentials // Proc. IEE. 1980. V. 127, Part B. No. 6. P. 368–374.

3. *Zhidkov E. P., Yuldashev O. I., Yuldasheva M. B.* An adaptive algorithm for computing a function on the Lipschitzian boundary of a 3D solid based on a prescribed gradient and its application in magnetostatics // Comp. Math. and Math. Phys. 2002. V. 42, No. 12. P. 1764–1779.

4. *Mitchell A. R., Wait R.* The finite element method in partial differential equations. M.: Mir, 1981 (in Russian).

5. Computational Magnetics / Ed. J. K. Sykulski. London: Chapman & Hall, 1995.

6. *Mihailov V. P.* Differential equations in partial derivatives. M.: Nauka, 1976 (in Russian).

7. *Zhidkov E. P., Yuldashev O. I., Yuldasheva M. B.* A projection method for solving linear problems with the divergence, curl operators and its application in magnetostatics //

Bulletin of Peoples' Friendship University of Russia, series Applied and Computer Mathematics. 2002. V. 1, No. 1. P. 79–86.

8. *Vodopianov A. S., Shishov Yu. A., Yuldasheva M. B., Yuldashev O. I.*. Computer models of dipole magnets of a series «VULCAN» for the ALICE experiment. JINR, E11-98-385. Dubna, 1998.

9. *Aleev A. N., Arefev V. A., Balandin V. P. et al.* EXCHARM spectrometer // Instrum. Exp. Tech. 1999. V. 42, No. 4. P. 481–492.